Research Square

Preprints are preliminary reports that have not undergone peer review.
They should not be considered conclusive, used to inform clinical practice,
or referenced by the media as validated information.

Low porosity and ultra-narrow linewidth in low temperature-sintered Ga-substituted In-LiZnTi ferrites for microwave integrated devices application

Yuan Shangxun
University of Electronic Science and Technology of China
Zhang Bo
University of Electronic Science and Technology of China
Wang Ziang
University of Electronic Science and Technology of China
Yang Yan
University of Electronic Science and Technology of China
Zhao Liting
University of Electronic Science and Technology of China
Guo Zhonghua
University of Electronic Science and Technology of China
Li Jie
lijie@uestc.edu.cn

University of Electronic Science and Technology of China

Research Article

Keywords: LiZnTi ferrite, Ga-substitution, Low porosity, Narrow linewidth

Posted Date: November 23rd, 2026

DOI: https://doi.org/10.21203/rs.3.rs-11632875/v1

License: This work is licensed under a Creative Commons Attribution 4.0 International License.
Read Full License

Additional Declarations: No competing interests reported.

Low porosity and ultra-narrow linewidth in low temperature-sintered Ga-substituted In-LiZnTi ferrites for microwave integrated devices application

Yuan Shangxun[1], Zhang Bo[1], Wang Ziang[1], Yang Yan[1,2], Zhao Liting[1], Guo Zhonghua[1], Li Jie[1,*]

[1] State Key Laboratory of Electronic Thin Film and Integrated Devices, University of Electronic Science and Technology of China, Chengdu, 610054, China

[2] College of Communication Engineering (College of Microelectronics), Chengdu University of Information Technology, Chengdu, 610225, China

Abstract: In this research, Ga-substituted In-LiZnTi ferrite materials ($Li_{0.44}Zn_{0.22}Ti_{0.12}Fe_{2.18-x}In_{0.04}Ga_xO_4$, x=0−0.15 with a step of 0.03) were prepared using solid state reaction method. Phase formation, microstructure, static magnetic performance, dielectric and gyromagnetic properties were systematically investigated. The results reveal that single phase spinel ferrite can be achieved at low sintering temperature (900 °C) by adding 0.75wt% Bi_2O_3 sintering aid. Owing to its small ionic radius, Ga^{3+}preferentially occupies the tetrahedral sites (A-sites) in LiZnTi ferrite without altering the spinel crystal structure. The intrinsic characteristics of Ga^{3+} together with bulk density directly govern the dielectric performance of the as-prepared ferrits. For the samples with x=0.06 ($Li_{0.44}Zn_{0.22}Ti_{0.12}Fe_{2.12}In_{0.04}Ga_{0.06}O_4$), the average grain size reaches 1.04 μm, and bulk density is 4.61g/cm^3. It exhibits outstanding comprehensive properties: σ_s = 61.81 emu/g, $4\pi M_s$ = 3682.14 Gs, μ' = 49.91 (at 1MHz), $\tan\delta_\mu$ = 0.002 (at 10 MHz) and narrow FMR linewidth ΔH = 202.1 Oe. The work demonstrates great application potential for microwave integrated devices.

Keywords: LiZnTi ferrite, Ga-substitution, Low porosity, Narrow linewidth

Introduction

LiZn ferrite is one of the key basic materials for high frequency microwave devices. It possesses merits such as excellent chemical stability, high saturation magnetization, and low ferromagnetic resonance linewidth [1]. Meanwhile, the ferrite material can be synthesized via low temperature sintering process with sintering aids, which meets the integration requirements of microwave systems. The inverse spinel structure of LiZn spinel ferrite has space group $Fd\bar{3}m$, where cations occupy the tetrahedral (A-sites) and octahedral (B-sites) [2]. Monovalent Li^{+} ion tends to induce valence imbalance in LiZn ferrite, therefore, Ti^{4+} ion is introduced to adjust valence balance and optimize magnetic properties of ferrites [3-5]. Ti^{4+} ion substitution can reduce magnetocrystalline anisotropy constant K_1 of LiZn ferrite, and lower the value of ferromagnetic resonance linewidth (about 264 Oe) [6]. Several metal ions have been chosen to substitute ions of LiZnTi ferrite and improve magnetic properties. Nb^{5+} ion substituted Li^{+} and Fe^{3+} ion of LiZnTi ferrite, and obtained a low ferromagnetic resonance linewidth (ΔH=337 Oe) [7]. Rare metal Gd^{3+} ion gave LiZnTi ferrite a high saturation magnetization ($4\pi Ms$=3940 Gs) and low ferromagnetic resonance linewidth (ΔH=270 Oe) [8]. Nano-LiZn ferrite was added into LiZnTi ferrite materials to lower sintering temperature, and with V2O5 sintering aid, the study showed a narrow ferromagnetic resonance linewidth of 197 Oe [9]. Our previous research, In^{3+} ion doped LiZnTi ferrites were successfully synthesized with a low temperature (920°C) using 2wt% Bi_2O_3 aid. When In^{3+} ion doped content was 0.06, $Li_{0.4}Zn_{0.3}Ti_{0.1}Fe_{2.14}In_{0.06}O_4$ had a high saturation magnetization of 4136.4 Gs and narrow ferromagnetic resonance linewidth of 240.09 Oe [10]. In the present study, Ga^{3+} ion was selected to substitute Fe^{3+} ion In-LiZnTi ferrite. This work aims to achieve high saturation magnetization, low magnetic loss and narrow ferromagnetic resonance linewidth for microwave integrated devices applications.

Experimental section

Based on pervious study and magnetic ferrite magnetism, the chemical composition of In-doped LiZnTi ferrite is $Li_{0.44}Zn_{0.22}Ti_{0.12}Fe_{2.18}In_{0.04}O_4$ (In-LiZnTi ferrite), and

Ga-substituted In-LiZnTi ferrite ($Li_{0.44}Zn_{0.22}Ti_{0.12}Fe_{2.18-x}In_{0.04}Ga_xO_4$，x=0−0.12 with a step of 0.03) materials were prepared by solid state reaction method using the high-purity (≥99%) raw materials Li_2CO_3, ZnO, TiO_2, Fe_2O_3, In_2O_3 and Ga_2O_3, provided by the Keshi Company. The raw materials were mixed in the required ratio and ball-milled for 12h with deionized water. The dried mixture was pre-sintered at 850° C for 2h. The powder was re-milled under identical conditions with 1.25wt% Bi2O3 as a sintering aid. Following another drying and sieving step, the powder was granulated with 12wt% polyvinyl alcohol (PVA) binder to obtain a particle size controlled between 0.15mm and 0.25mm. The particles were pressed into green bodies of the desired shape for characterization and testing under a uniaxial pressure of 10MPa. The samples were sintered at 900° C for 4h and then naturally cooled to room temperature.

The phase formation of the samples was characterized by X-ray diffraction (XRD, Ultima IV, Rigaku, Japan) with Cu-Kα radiation (λ=1.54 Å), scanned from 20° to 70° with a step size of 0.01. The microstructure of the samples was observed via scanning electron microscopy (SEM, LMS Quantax 200). The bulk density of the samples was determined using Archimedes′ principle (AND GF-300, Japan). The magnetic hysteresis loops were measured using a vibrating sample magnetometer (VSM, Lakeshore 7404, USA) under a magnetic field of ±5000Oe. The complex magnetic permeability (μ′ and μ″) was obtained using an Agilent Network Analyzer (E991B). The ferromagnetic resonance linewidth (ΔH) of the spherical samples with a diameter of approximately 1mm was measured by a vector network analyzer (8722ES, Agilent, USA) via TE_{106} cavity perturbation (9.56 GHz). All measurements were performed at room temperature.

Results and discussion

Fig.1 illustrates the XRD patterns and crystal structure model of the $Li_{0.44}Zn_{0.22}Ti_{0.12}Fe_{2.18-x}In_{0.04}Ga_xO_4$ ferrite materials. As shown in Fig. 1(a), all samples are pure spinel ferrite phase, and their diffraction peaks (220), (311), (422), (400), (511) and (400) are well-defined, and no impurity peaks are observed. This indicates

that Ga^{3+} ion substitution does not alter the crystal structure of In-LiZnTi ferrite. As observed in the magnified XRD pattern (Fig. 1(b)), the strongest diffraction peak (311) shifts toward high 2θ angles as x increases, demonstrating that Ga^{3+} ion substitution reduces the unit cell volume. Based on XRD pattern, the lattice parameters (a), unit-cell volumes (V) and X-ray theoretical density (ρ_x) results are summarized in Table 1. As the substitution level increase, the lattice constant gradually decreases from 8.3589 Å to 8.3374 Å, which is consistent with the shift in the diffraction peaks observed in the XRD patterns. Meanwhile, X-ray theoretical density (ρ_x) exhibits a mild upward trend, increasing from 4.86g/cm^3 to 4.89g/cm^3. The preferred lattices of Ga^{3+} and In^{3+} within LiZnTi spinel lattice are presented in Figure 1(c). The reduction in lattice constant is primarily attributed to the difference in ionic radius between doped Ga^{3+} ion and the replaced Fe^{3+} ion. The ionic radius of Ga^{3+} ion is 0.62 Å, compared with 0.74 Å for Fe^{3+} ion [11]. Moreover, the Fe-O bond length in the tetrahedral site is 1.87 Å, whereas the Ga-O bond length is 1.83 Å. Consequently, substitution of Fe^{3+} by Ga^{3+} ion leads to a decreasing trend in the lattice constant. Additionally, upon substitution of Fe^{3+} by Ga^{3+}ion, Ga^{3+} possesses a higher relative atomic mass (M_{Ga} = 72.63) than Fe (M_{Fe} = 55.85). At an identical molar doping level, the increased formula mass of the ferrite, together with the contracted unit cell volume (as shown in Table 1), leads to an enhancement in the theoretical density.

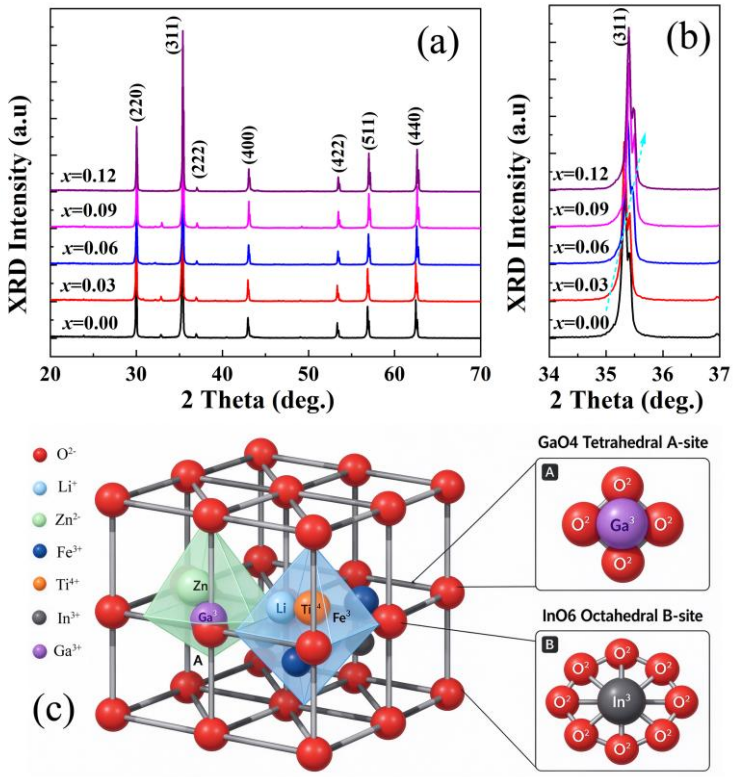

Fig. 1 XRD patterns and crystal structure model of samples. (a) XRD patterns of Ga-substituted In-LiZnTi ferrite, (b) Magnified view of the XRD patterns in the 2θ range of 34°-37°, (c) Crystal structure model of Ga-substituted In-LiZnTi ferrite.

Table 1 Refined lattice parameters (a), unit-cell volumes (V) and X-ray theoretical density (ρ_x) of Ga-substituted In-LiZnTi ferrite

	x=0.00	x=0.03	x=0.06	x=0.09	x=0.12
Lattice constant a (Å)	8.3589	8.3512	8.3445	8.3401	8.3374
unit-cell volume V ($Å^3$)	584.05	582.43	581.03	580.11	579.55
XRD theoretical density ρ_x (g/cm^3)	4.86	4.87	4.88	4.89	4.89

Figure 2 shows the SEM microstructures of Ga-substituted In-LiZnTi ferrites as well as the elemental mapping of Fe, In and Ga of the x=0.06 sample. As x=0.00 (as shown in Figure 2(a)), the grains are relatively homogeneous and no oversized grains are observed. As the Ga^{3+} ion substituted level increases, large grains gradually develop in the ferrite samples, and such large grains are clearly visible at x=0.09. This suggests that Ga^{3+} substitution can enhance grain boundary bonding and favor the

growth of larger grains. Elemental mapping was performed with x=0.06 (Figure 2(c)). Figure 2(f) and 2(g) show the distribution of Fe and In element, respectively, while Figure 2(h) presents the Ga distribution. In spinel ferrite, both In^{3+} and Ga^{3+} ions occupy tetrahedral sites [12]. The element mapping results shows Ga^{3+} substitution dos not alter distribution of Fe and In elements, indicating no site competition between Ga and In elements at tetrahedral positions. Meanwhile, the uniform Ga distribution in Figure 2(h) demonstrates that Ga^{3+} ions are incorporated homogeneously into the tetrahedral lattice sites without agglomeration.

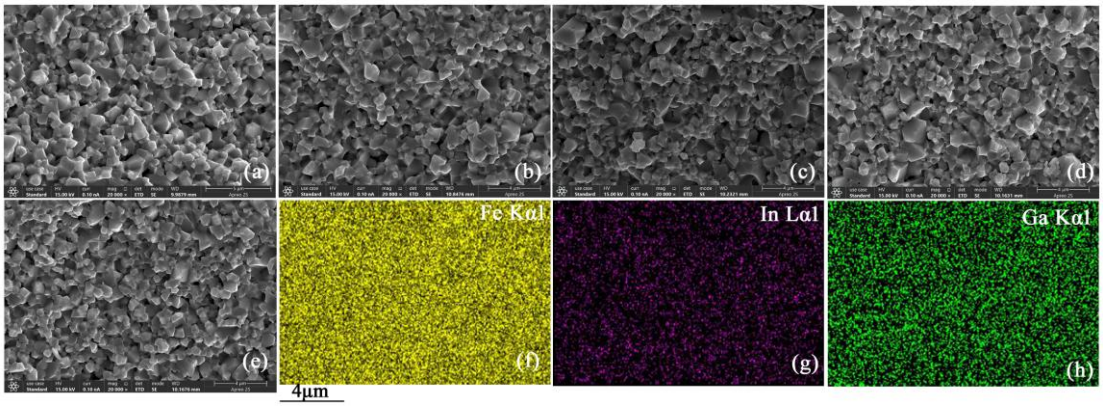

Fig.2 SEM and EDS images of Ga-substituted In-LiZnTi ferrite. (a) x=0.00, (b) x=0.03, (c) x=0.06, (d) x=0.09, (e) x=0.12, (f) Fe element distribution mapping of x=0.06 samples, (g) In element distribution mapping of x=0.06 samples, (h) Ga element distribution mapping of x=0.06 samples

Figures 3(a-e) show the grain size distribution and average grain size of the samples with different Ga^{3+} ion substituted contents. The average grain sizes are in good agreement with the SEM observation. As the substituted level x increases, the average grain size first increases and then decreases: in rises from 0.95 μm for the x=0.00 sample to 1.04 μm for the x=0.06 sample, and subsequently falls to 0.96 μm. In terms of grain size distribution, 86.58% of grains fall within the range of 0.5 μm-1.5 μm for the x=0.00 sample. As x increases to 0.12, the proportion of grains in the 0.5 μm-1.5 μm range reaches 89.91%.The overall variation in grain size remains modest, which is mainly attributed to the low Ga^{3+} ion substituted content and the weak influence of Ga incorporation on the unit cell. The decrease in average grain size for the x=0.09 and x=0.12 samples can be ascribed to the coexistence of abnormally large and fine grains

at higher substitute levels, leading to broadened and non-uniform grain size distribution.

Figure 3(f) shows the bulk density of ferrites with different Ga^{3+} ion substitution. As x increases from 0.00 to 0.12, the bulk density of the material first rises from 4.645 g/cm^3 to 4.745 g/cm^3 (x=0.06), and then decreases to 4.682 g/cm^3. The bulk density is mainly determined by the intrinsic structure and densification of the material. When the substituting level increases from 0.00 to 0.06, the increased grain size and improved grain homogeneity are the primary factors contributing to the density enhancement. At high substituting levels (x≥0.09), large grains induce more pores between grains, resulting in a decrease in measured density. The porosity *P* was calculated using Equation (1), and the results are presented in Figure 3(f) [13]:

$$P = \frac{(\rho_x - \rho_b)}{\rho_x} \times 100\% \quad (1)$$

The porosity *P* exhibits a trend of first decreasing and then increasing: it declines from 4.42% for the x=0.00 sample to 2.81% for the x=0.06 sample, and then rises to 4.25% for the x=0.12 sample. The porosity exerts a notable influence on the magnetic loss, especially the ferromagnetic resonance linewidth of the ferrites.

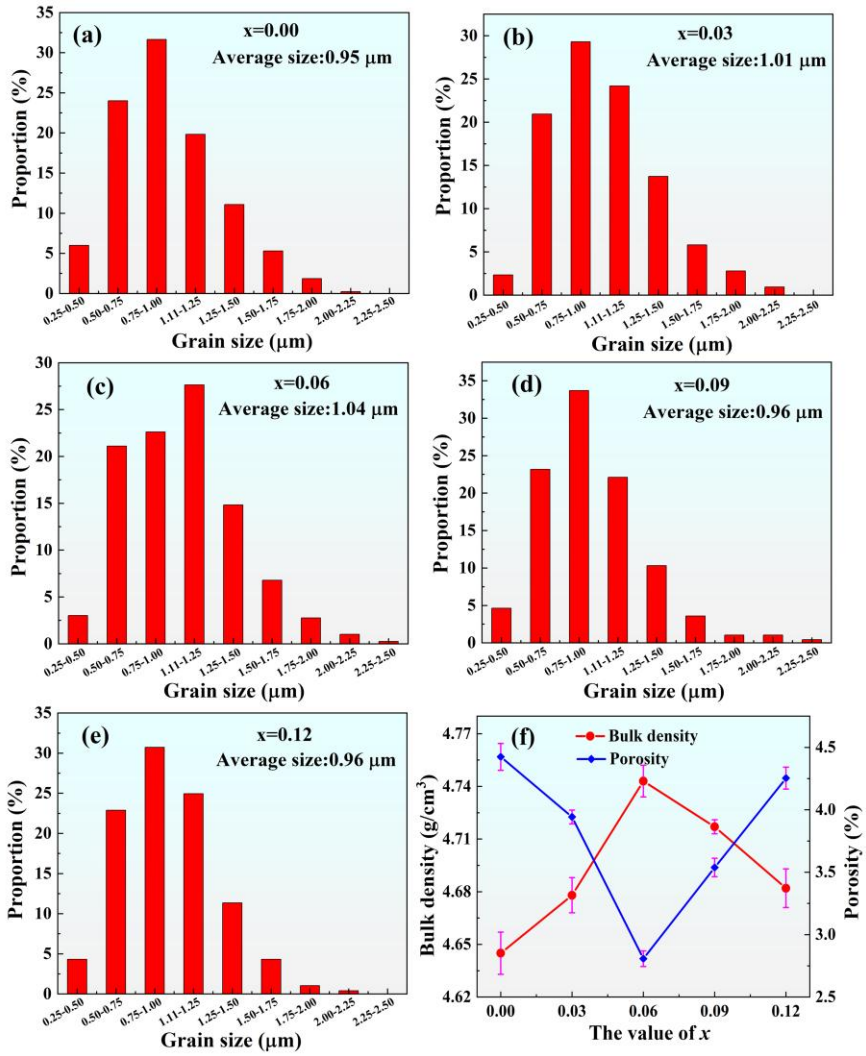

Fig.3 Grain size distribution, average grain size, bulk density and porosity of of Ga-substituted In-LiZnTi ferrite. (a-e) Grain size distribution and average grain size of samples, (f) Bulk density and porosity of samples

The room temperature magnetic hysteresis loops of Ga^{3+} ion substituted ferrites are shown in Figure 4(a), and Figure 4(b) illustrates the variations in specific saturation magnetization (σ_s), saturation magnetization ($4\pi M_s$) and coercivity (H_c). It can be seen from Figure 4(a) that all ferrite samples exhibits soft magnetic characteristic and reach magnetic saturation under an applied field of 2000 Oe. As x increases, the value of σ_s rises from 61.25 emu/g to 62.55 emu/g. For ferrites, the specific saturation magnetization is related to the total magnetic moment and superexchange interaction [14]. In Ga^{3+} ion substituted In-LiZnTi ferrites, Ga^{3+} with small ionic radius tends to

form covalent bonds with Sp^3 hybrid orbitals [15]. Its spatial coordination features a high probability of electron distribution along the directions from the center of the tetrahedron to the four vertices, so Ga^{3+} ion preferentially occupies the A-sites of the spinel ferrite. Considering the site preference of cations in In-LiZnTi ferrite, the cation distribution of the ferrite can be expressed by Equation (2):

$$(Zn_{0.22}^{2+}In_{0.04}^{3+}Ga_{x}^{3+}Fe_{0.74-x}^{3+})[Li_{0.44}^{1+}Ti_{0.12}^{4+}Fe_{1.44+x}^{3+}]O_{2}^{2-} \quad (2)$$

Where ( ) denotes the tetrahedral A sites and [ ] represents the octahedral B sites of the spinel ferrite. In can be observed form Equation (2) that as the Ga content increases, the concentration Fe^{3+} at the A sites decreases continuously, while that of Fe^{3+} at the B sites increases gradually. Since the remaining cations are all non-magnetic metal ions, the total magnetic moment (M_{total}) of the ferrite can be expressed by Equation (3):

$$M_{total} = |M_{B-site} - M_{A-site}| = |(1.44 + x) - (0.74 - x)| \times 4.9\mu B = (0.7 + 2x) \times 4.9\mu B \quad (3)$$

Therefore, the total magnetic moment of the ferrite increases with rising Ga^{3+} ion substitute content, which contributes to an enhancement in the specific saturation magnetization. This accounts for the increase in specific saturation magnetization. In addition, the Fe^{3+}-O^{2-}-Fe^{3+} superexchange interaction between the A and B sites is the strongest in spinel ferrites [16]. Nevertheless, increasing Ga^{3+} content reduces the Fe^{3+} fraction on A sites and raises the Fe^{3+} fraction on B sites, which weakens the A-B superexchange interaction. This is the reason for the small rising amplitude of the specific saturation magnetization.

In microwave devices, saturation magnetization ($4\pi M_s$) us a core parameter that governs the operating frequency band, applied magnetic field and power capacity of microwave devices [17, 18]. It directly affects the loss, bandwidth and design feasibility of the devices. Therefore, in this work, the value of $4\pi M_s$ was calculated via Equation based on the measured specific saturation magnetization and bulk density:

$$4\pi M_s = 4 \times \rho_b \times \sigma_s \quad (4)$$

The results are presented in Figure 4(b), as the value of x increases, the $4\pi M_s$ rises from 3575.15 Gs (x=0.00) to 3682.14 Gs (x=0.06), and subsequently decreases to 3678.31 Gs (x=0.12). The variation in saturation magnetization mainly originates

from the intrinsic magnetic properties and density of the material. For the same composition, higher density and lower porosity exert a positive effect on enhancing the saturation magnetization.

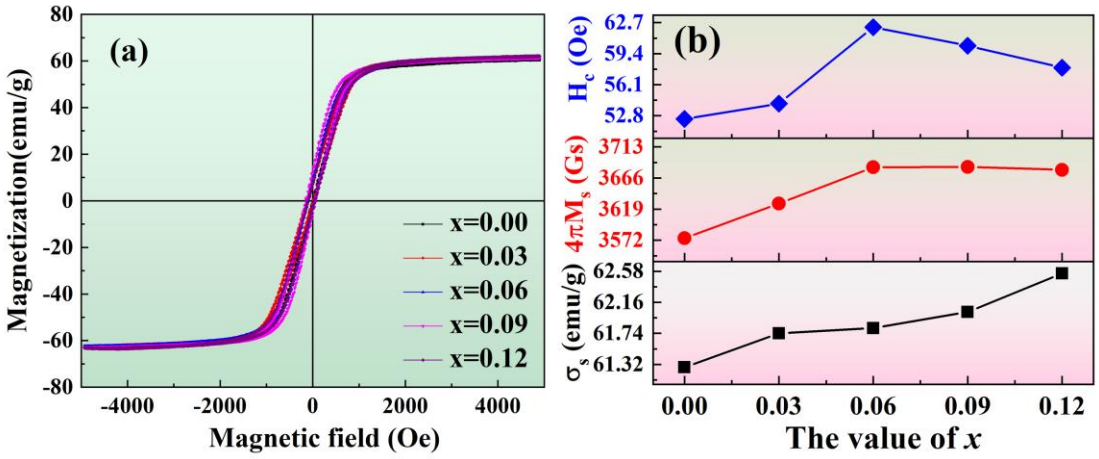

Fig.4 Magnetic hysteresis loops and the magnetic parameters of Ga^{3+} ion substituted ferrites. (a) Magnetic hysteresis loops of samples, (b) the magnetic parameters of samples

Figure 4(b) presents the variation in coercivity (H_c) as a function of x. As x increases, the coercivity rises from 52.45 Oe (x=0.00) to 62.21 Oe (x=0.06), and then decreases to 57.91 Oe (x=0.12). For ferrites, coercivity is one of the key parameters governing hysteresis loss [19]. It is mainly affected by grain size, magnetocrystalline anisotropy, magnetic domain wall and porosity. In this work, at low Ga^{3+} ion substitute level ($x \leqslant 0.06$), Ga^{3+} ions occupy the A sites and substitute for Fe^{3+} ions. This substitution reduces the Fe^{3+} concentration at A sites while increasing the Fe^{3+} ion content at B sites, weakening the A-B superexchange interaction and raising the effective magnetocrystalline anisotropy constant K_1 [20]. Coercivity is positively correlated with magnetocrystalline anisotropy, which accounts for the increase in coercivity. In addition, slight Ga^{3+} ion substitution leads to a slow growth of grain size and a reduction in porosity. Minor grain boundary segregation introduces increased microinternal stress, which hinders domain wall displacement and further elevates the coercivity.

As the Ga^{3+} ion substitution level further increases ($x \geqslant 0.06$), more Fe^{3+} ions at A site are substituted, and the A-B superexchange interaction is further weakened. The

compensation mode of magnetic moments between the A and B sublattices changes, and the overall effective magnetocrystalline anisotropy gradually decreases. Combined with the increase in specific saturation magnetization, the coercivity starts to decline. Meanwhile, high substitution level induces non-uniform grain size and the formation of large grains. The increased porosity releases part of the internal stress, which further promotes the reduction of coercivity.

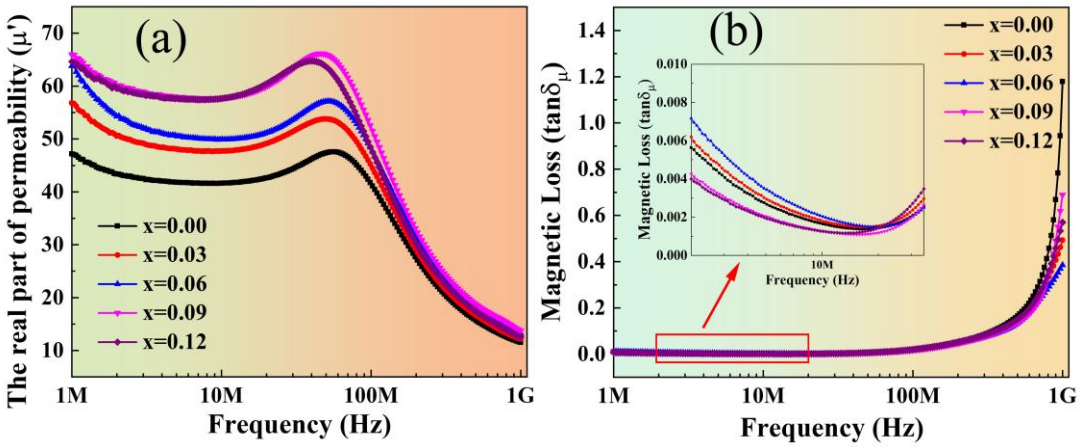

Fig. 5 Real part of permeability (μ′) and magnetic loss (tanδ_μ) of Ga-substituted In-LiZnTi ferrites. (a) The real part of permeability of the samples, (b) magnetic loss of the samples

Real part of permeability (μ′) and magnetic loss (tanδ_μ) of Ga-substituted In-LiTiZn ferrites were measured over the frequency range from 1 MHz to 1 GHz, and the results are presented in Figure 5. Figure 5(a) shows the real part of permeability, while Figure 5(b) displays the magnetic loss. As illustrated in Figure 5(a), the real part permeability exhibits an upward trend with increasing Ga^{3+} substitute content x, rising from 41.60 for x=0.00 sample to 57.77 for x=0.09 sample. The value of μ′ of the x=0.09 and x=0.12 samples are nearly identical. For ferrite, the real permeability originates mainly from two magnetization mechanism: domain wall displacement and magnetic moment rotation. According to Equation (5), the real permeability is related to the specific saturation magnetization (σ_s), magnetocrystalline anisotropy constant (K_1) and impurity factor (β) of the materials [21].

$$\mu' \propto \frac{\sigma_s^2}{K_1 \beta} \tag{5}$$

The increase in specific saturation magnetization with rising Ga^{3+} substitution is the

dominant factor for the enhanced permeability. Moreover, at low substitution levels, the improved densification and reduced porosity weaken the effects of internal stress and other defects. Uniform grains lower the resistance to domain wall displacement, and sustain the upward trend of permeability. For $x \geqslant 0.06$, the A-B superexchange interaction is continuously weakened, and the magnetic moment balance between the A and B sublattices is altered [22]. The reduction in the magnetocrystalline anisotropy constant K_1 facilitates a further increase in permeability. Meanwhile, large grains emerge in the ferrites at substitution levels of x=0.09 and x=0.12, which increases the number of domain walls and raises the resistance to domain wall motion. Consequently, the growth of permeability slows down.

Figure 5(b) shows the magnetic loss results of the samples. It can be observed that the loss remains at a low levels below 0.01 as the Ga^{3+} substitution content increases. For ferrites operating in the microwave frequency band, magnetic loss generally consists of hysteresis loss, eddy current loss and domain wall relaxation loss [23]. Within the measured frequency range of 1 MHz to 1 GHz, the total magnetic loss is dominated by hysteresis loss and domain wall relaxation loss. The evolution of hysteresis loss is closely associated with the magnetocrystalline anisotropy constant. At low substitution levels, the A-B superexchange interaction weakens and K_1 rises, leading to an increase in hysteresis loss. At high substitution levels, K_1 decreases, and hysteresis loss is reduced. Accordingly, the inset in Figure 5(b) indicates that the variation trend of magnetic loss is correlated with hysteresis loss. In addition, porosity and grain homogeneity are critical factors affecting domain wall relaxation loss. Lower porosity and better grain homogeneity both contribute to reduced domain wall relaxation loss. In summary, the magnetic loss of the ferrite is a combined result of magnetocrystalline anisotropy and grain morphology.

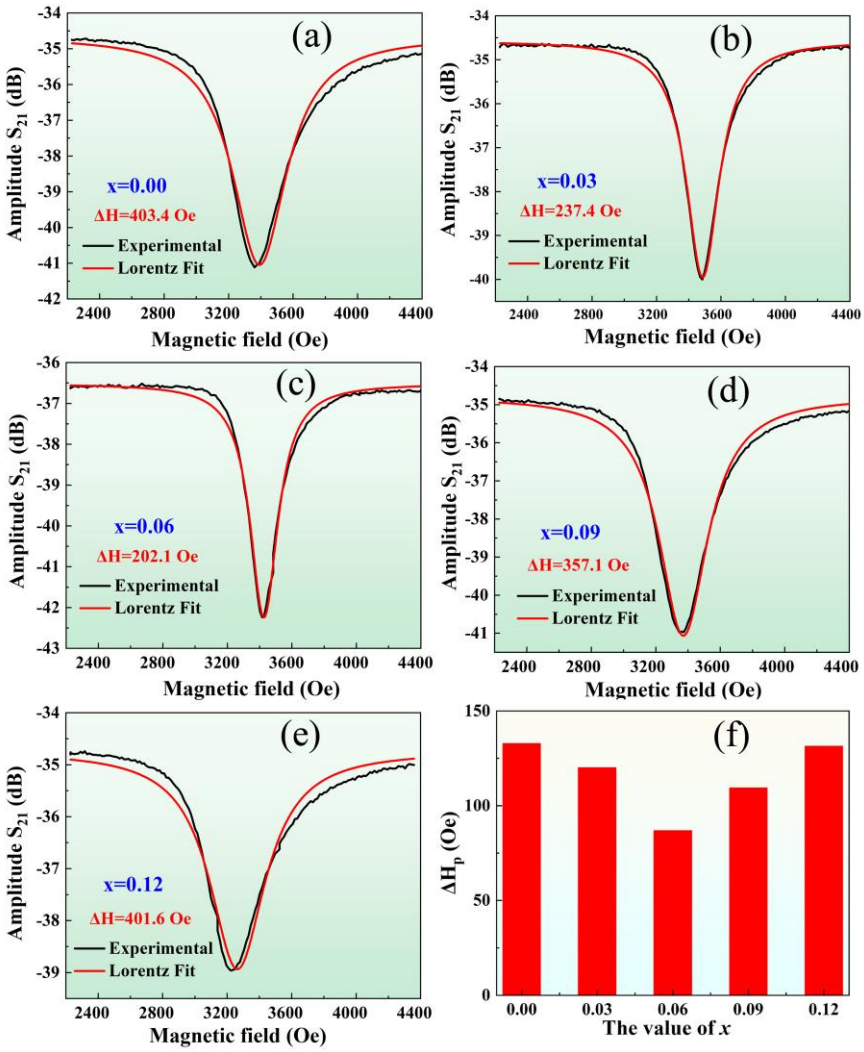

Fig.6 ferromagnetic resonance linewidth (ΔH) and porosity linewidth (ΔH_p) of Ga^{3+} ion substituted In-LiZnTi ferrite. (a-e) the value of ΔH, (f) the value of ΔH_p

Figure 6 shows the ferromagnetic resonance linewidth (ΔH) of Ga^{3+} ion substituted In-LiZnTi ferrite measured at 9.56 GHz. As x increases, the value of ΔH decreases from 403.4 Oe (x=0.00) to 202.1 Oe (x=0.06), and then rises to 401.6 Oe (x=0.12). For polycrystalline ferrite, the main contributions to the ferromagnetic resonance linewidth can be expressed by Equation (6) [24]:

$$\Delta H = \Delta H_i + \Delta H_a + \Delta H_p + \Delta H_{inc} \quad (6)$$

where ΔH_i is the intrinsic linewidth, ΔHa is the magnetocrystalline anisotropy linewidth,, ΔH_p is the porosity linewidth, and ΔHinc is the second phase linewidth. In this work, the ferromagnetic resonance linewidth is governed primarily by

magnetocrystalline anisotropy, superexchange interaction, microstructure and porosity. As x increases from 0.00 to 0.06, the incorporation of Ga^{3+} ion first reduces superexchange interaction of the sample, which contributes to a narrow linewidth. Second, appropriate Ga^{3+} ion substitution improves sintering densification, yields uniform grain size and reduces overall porosity, further lowering the value of ΔH. While the magnetocrystalline anisotropy constant shows an increasing trend in this doping series, the ferromagnetic resonance linewidth is markedly reduced owing to the competition among multiple influencing factors. When x is further increased up to 0.12, the increase in linewidth originates mainly from the imbalance of magnetic moments on the A and B sublattices and the weakened superexchange interaction, together with the emergence of abnormally larger grains and elevated porosity. Large grains induce local compositional segregation, which spreads the distribution of resonance fields and increases the inhomogeneous linewidth. Among all linewidth contributions, the porosity term ΔH_p has long been a key research focus. In spinel ferrite, ΔH_p calculated by Equation (7) is plotted in Figure 6(f) [25]:

$$\Delta H_p = 0.85 \times 4\pi M_s \times P \quad (7)$$

The calculated results reveal that ΔHp varies with porosity: it first decreases from 132.85 Oe to 86.83 Oe at x=0.06 and subsequently increases to 131.43 Oe. The porosity linewidth accounts for 30%~50% of the total linewidth of the sample, demonstrating that reducing porosity is one of the effective routes to minimize the resonance linewidth. A lower ferromagnetic resonance linewidth corresponds to smaller insertion loss and superior transmission performance for microwave devices.

Conclusion

In this study, Ga^{3+}-substituted In-LiZnTi ferrites were synthesized via the solid state reaction method with 0.75wt% sintering aid at a low sintering temperature of 900 °C. Ga^{3+} ion substitution does not alter the spinel phase of In-LiZnTi ferrite, yet it exerts a remarkable influence on the microstructure. Appropriate substitute content improves grain uniformity and reduces porosity. In term of magnetic properties, Ga^{3+} ion substitution and its ionic occupancy sites modulate the magnetic moment,

magnetocrystalline anisotropy, superexchange interaction and interlattice magnetic moment balance of the material, thereby tailoring its magnetic performance. At a substitution level of 0.06, the sample achieves a high saturation magnetization ($4\pi M_s$=3862.14 Gs), low magnetic loss (tan$\delta\mu$=0.002) and narrow ferromagnetic resonance linewidth (ΔH=202.1 Oe). The optimized magnetic properties render the ferrite promising for intergrated microwave devices with respect to operating frequency, insertion loss and operational bandwidth.

Acknowledgement

This work was supported by the National Natural Science Foundation of China. (Nos. 52602477 and 62271106).

References

[1] T.N. Singh, M. Maisnam, Studies of the frequency and temperature dependence of the electromagnetic properties of Ti-substituted Li-Zn-Mn spinel ferrite, Ceramics International 52 (8) (2026) 10864-10881.

[2] S. Neeradi, G. Vinod, L.R. Kotha, Exploring the impact of Mn-Dy co-doping on the structural, optical, spectral, magnetic characteristics and photocatalytic activity of $CoFe_2O_4$ nano-ferrites, Appl Phys a-Mater 132 (3) (2026) 147.

[3] J.L. Liu, F. Xu, Y. Yang, Y. Ren, G.X. Liu, B. Dai, Low-temperature synthesis of uniform and compact LiZnTi ferrite via a synergistic method, Journal of Alloys and Compounds 1057 (2026) 186775.

[4] M.C. Yang, L.J. Jia, L. Xu, P.H. Yi, Y. Shen, W.L. Fu, Z.H. Chen, Zn-Ti co-substituted LiZn microwave ferrites: Sintering characteristics and gyromagnetic properties, Journal of Magnetism and Magnetic Materials 600 (2024) 172171.

[5] Y. Gao, Z. Wang, Microwave absorption and electromagnetic interference shielding properties of Li-Zn ferrite-carbon nanotubes composite, Journal of Magnetism and Magnetic Materials 528 (2021) 167808.

[6] Q.S. Yin, Y.L. Liu, Q. Liu, Y. Wang, J.F. Chen, H.X. Wang, C.S. Wu, H.W. Zhang, Investigation on Ti^{4+} substitution LiZn ferrite with FMR linewidth at Ku band, Mater Res Express 6 (3) (2019) 036108.

[7] R. Tang, C.S. Wu, L. Zhao, C. Du, C. Zhang, Q. Liu, T.P. Liang, Y.M. Lai, Microstructure, magnetic, and gyromagnetic properties of Nb^{5+} ion substituted LiZnTi ferrites, Ceramics International 51 (10) (2025) 13111-13117.

[8] R. Tang, C.S. Wu, L. Zhao, C. Du, C. Zhang, J.J. Chen, L.J. Chen, Q. Liu, Y.M. Lai, Synthesis of Gd^{3+}-substituted LiZnTi ferrites with enhanced magnetic and gyromagnetic properties, Journal of the

American Ceramic Society 109 (1) (2025) e70236.
[9] H.W. Yang, M.J. Guo, F. Xu, Y.L. Liao, Y. Ren, G.X. Liu, H.L. Lai, B.C.W. Sun, B. Dai, Microstructure and gyromagnetic properties of low-sintered LiZnTi ferrite doped with nano-LiZn and V2O5 additives, Journal of Alloys and Compounds 947 (2023) 169516.
[10] J.Y. Yuan, J. Li, Y. Xiao, X.Y. Zhu, S.Y. Wang, Y. Yang, J.L. Zou, Y.C. Yan, Enhanced microwave gyromagnet and dielectric properties of In-doped LiZnTi spinel ferrite for high frequency device application, Ceramics International 51 (25) (2025) 47068-47075.
[11] E. Martínez-Aguilar, H. Hmok, J.M. Siqueiros, R. López-Juárez, Effect of single and mixed Bi, Ga doping on the magnetic properties of $Y_3Fe_5O_{12}$, Computational Materials Science 214 (2022) 111752.
[12] S. Verma, M. Singh, Study of Structural and Magnetic Properties of In^{3+} Substituted Mg-Mn-Ni Spinel Ferrites, Solid State Physics: Proceedings of the 55th DAE Solid State Physics Symposium 2010, 1349 (2011) 1137-1138.
[13] S. Salam, A. Sarmah, I. Soibam, Zinc substituted nickel-copper ferrite ceramics: A study on structural, dielectric and magnetic properties, Journal of Materials Science- Materials in Electronic 37 (15) (2026) 1188.
[14] C. Zhang, X.Y. Wu, C.S. Wu, L. Zhao, C. Du, R. Tang, Improved microstructure and gyromagnetic properties of NiCuZn microwave ferrites by adopting Zr^{4+} substitution, Ceramics International 52 (12) (2026) 20066-20072.
[15] S. Ali, O.M. Hemeda, F. Elhussiny, M.H. Mahgoub, S. Mohammed, A. Elmekawy, Structural, optical, and magnetic characterization of Cu-Zn-Ni spinel ferrite nanoparticles with antibacterial potential, Scientific Reports 16 (1) (2026) 3053.
[16] P.C. Patil, A.A. Gaikwad, P.K. Gaikwad, R.H. Kadam, S.E. Shirsath, J.J. Chamargore, Cation distribution-mediated structural expansion and magnetic softening in Ce-Y Co-substituted Ni-Zn ferrite nanomaterials, Chemistryselect 11 (20) (2026) e73503.
[17] X.G. Hu, J.C. Su, Y. Ying, M. Li, R. Li, J. Cheng, S.T. Wu, M. Guo, H.C. Zhang, Q. Wang, F.Z. Liu, Research on the power-handling capability of latching non-reciprocal ferrite phase shifters, IEEE Transactions on Magnetic 62 (2) (2026) 4000312.
[18] Y.N. Zhao, Y.J. Li, Z.Y. Zhou, R.C. Peng, S.K. Zhu, M.T. Yao, B. Peng, Y.F. Zhao, Y.X. Cheng, B. Tian, Z.Q. Hu, Z.G. Ye, Z.D. Jiang, M. Liu, Low-damping flexible Y3Fe5O12 thin films for tunable RF/microwave processors, Mater Horiz 7 (6) (2020) 1558-1565.
[19] G.J. Zou, X.M. Luo, G.W. Gan, K. Liu, Z.L. Zheng, Optimized magnetic and dielectric properties of CoY ferrite for UHF antenna applications achieved via Cd^{2+} ion doping, Ceramics International 52 (10) (2026) 14875-14882.
[20] M.R. Yadav, M. Sudheer, V.L.N.B.G. Tiruveedhi, Tailoring structural and magnetic, and electrical properties of Al^{3+}-Cr^{3+} co-substituted Ni-Zn ferrites for high-frequency and EMI applications, Inorgainc Chenistry Communications 188 (2026) 116484.
[21] I. Soudani, N. Mustapha, M. Hjiri, Effect of divalent cation substitution (M = Mn, Ni, Mg, Cu) on the structural, magnetic and electrical properties of MFe_2O_4 spinel ferrites, Rsc Advances 16 (28) (2026) 25515-25528.

[22] K.V. Shikare, H. Ferjani, K.K. Patil, Y.G.A. El-Reash, T.A. Yousef, S.D. Sutar, M. Ayyar, H. Elhouichet, V.M. Khot, H. Koheil, B.E. Keshta, R.P. Patil, Specific absorption rate of magnetic Ni-Zn-Mg mixed ferrite nanoparticles for magnetic hyperthermia, Journal of Materials Science-Materials in Electronics 37 (11) (2026) 821.

[23] M.A. Khalid, G.M. Mustafa, I. Asghar, M.R. Saleem, A.A. Al-Kahtani, Evaluation of temperature-dependent studies of holmium-doped Cu-Co spinel ferrites-based graphene composites, Journal of Materials Science- Materials in Electronics 37 (1) (2026) 85.

[24] Y. Xiao, J. Li, Y. Yang, Y.D. Lei, Y.L. Ma, Y.L. Liu, Synergistic modulation of magnetic and dielectric properties in high-Bi-content garnet ferrites, Journal of the European Ceramic Society 45 (15) (2025) 117639.

[25] H.Y. Zhang, Q.F. Li, X.A. Jiang, C.J. Wu, K. Sun, Z.W. Lan, Z. Yu, Power capacity enhancement and loss reduction induced by limited solid solubility of Ho3+rare-earth substitution in NiCuZn spinel ferrites, Journal of Advanced Ceramics 13 (10) (2024) 1655-1665.